Generalized model of the microwave auditory effect

2009 Phys. Med. Biol. 54 4037

(http://iopscience.iop.org/0031-9155/54/13/006)

IOP PUBLISHING PHYSICS IN MEDICINE AND BIOLOGY

Phys. Med. Biol. **54** (2009) 4037–4049 doi:10.1088/0031-9155/54/13/006

Generalized model of the microwave auditory effect

N M Yitzhak, R Ruppin and R Hareuveny

Radiation Safety Division, Soreq NRC, Yavne 81800, Israel

E-mail: ruppin@ soreq.gov.il

Received 21 January 2009, in final form 7 May 2009
Published 5 June 2009
Online at stacks.iop.org/PMB/54/4037

Abstract

A generalized theoretical model for evaluating the amplitudes of the sound waves generated in a spherical head model, which is irradiated by microwave pulses, is developed. The thermoelastic equation of motion is solved for a spherically symmetric heating pattern of arbitrary form. For previously treated heating patterns that are peaked at the sphere centre, the results reduce to those presented before. The generalized model is applied to the case in which the microwave absorption is concentrated near the sphere surface. It is found that, for equal average specific absorption rates, the sound intensity generated by a surface localized heating pattern is comparable to that generated by a heating pattern that is peaked at the centre. The dependence of the induced sound pressure on the shape of the microwave pulse is explored. Another theoretical extension, to the case of repeated pulses, is developed and applied to the interpretation of existing experimental data on the dependence of the human hearing effect threshold on the pulse repetition frequency.

1. Introduction

The absorption of pulsed microwave energy can produce an auditory sensation in human beings, which manifests itself as a clicking, buzzing or hissing sound. Although the hearing effect has been experienced by radar operators since the introduction of radar systems, the first systematic experimental study of this effect has been performed by Frey (1961, 1962). The thermoelastic expansion mechanism, first proposed by Foster and Finch (1974), is responsible for the hearing effect. The absorption of the microwave energy produces a rapid thermal expansion, resulting from a small temperature rise, of the order of 10^{-6} °C. This launches a thermoelastic wave of acoustic pressure that travels to the inner ear. Detailed reviews of the results of human, animal and modelling studies, which support this explanation of the hearing effect, have been presented by Chou *et al* (1982) and Elder and Chou (2003).

A mathematical technique for solving the thermoelastic equation of motion analytically for a homogeneous spherical head model has been presented by Lin for two types of boundary conditions: (a) free boundary, so that the normal stress vanishes at the sphere surface (Lin

1977a); (b) rigidly constrained boundary, so that the displacement vanishes at the sphere surface (Lin 1977b). Lin has used a specific spherically symmetric heating pattern, which is peaked at the sphere centre. The same technique has been employed by Shibata *et al* (1986) for a modified specific heating pattern, which was also spherically symmetric and centrally peaked. Here we present a general analytic solution, which is applicable to an arbitrary spherically symmetric heating pattern. We demonstrate that for the specific, centrally peaked heating patterns treated before, our generalized solution reduces to the known results. Our generalized solution enables us to investigate other cases, such as that of a surface concentrated heating pattern, which has not been treated before. This is of practical interest, since for high enough frequencies the absorption of the electromagnetic energy occurs mainly near the surface of the sphere.

Moreover, in all previous theoretical models only a single rectangular microwave pulse was assumed. Here we extend the treatment and examine the effect of using other pulse shapes (half-sine and sawtooth). We also treat the case of repeated pulses, and investigate the dependence of the threshold for the effect on the pulse repetition rate.

We note that the thermoelastic expansion mechanism is of interest not only in relation to the hearing effect. It has recently been applied as an ingredient of a new imaging technique, called thermoacoustic tomography, in which pulsed microwave radiation is used to irradiate the sample. Absorbed microwave energy causes thermoelastic expansion, which induces acoustic waves that propagate in the sample. These waves are detected by an ultrasonic transducer that is scanned around the object to reconstruct the microwave energy deposition in the tissue (Ku and Wang 2000, Jin and Wang 2006).

2. Theoretical formulation

2.1. Temperature rise

The most general spherically symmetric absorption pattern inside a sphere of radius a can be written in terms of its Taylor expansion in the form

$$I(r,t) = f(t)\sum_{n=0}^{\infty} I_n \left(\frac{r}{a}\right)^n. \tag{1}$$

Here $I(r, t)$ is the absorbed power density at radial distance r from the sphere centre at time t, I_n is the nth Taylor expansion coefficient and $f(t)$ represents the pulse shape (usually assumed to be rectangular). The temperature rise $\theta(r, t)$ resulting from the absorption of the electromagnetic wave follows from the heat conduction equation (Carslaw and Jaeger 1959)

$$\nabla^2\theta(r,t) - \frac{1}{\kappa}\frac{\partial\theta(r,t)}{\partial t} = -\frac{I(r,t)}{K}, \tag{2}$$

where κ and K are the thermal diffusivity and conductivity of brain matter, respectively. The temperature decay processes are slow, and can be neglected for the short pulse durations considered here (tens of microseconds). Thus, the spatial derivatives in equation (2) can be neglected, reducing it to the form

$$\frac{\partial\theta(r,t)}{\partial t} = \frac{\kappa}{K} I(r,t). \tag{3}$$

This can be integrated, yielding

$$\theta(r,t) = \frac{1}{\rho c_h} F_t(t)\sum_{n=0}^{\infty} I_n \left(\frac{r}{a}\right)^n. \tag{4}$$

Here ρ and c_h are the density and specific heat of brain matter, respectively, and $\rho c_h = K/\kappa$.

$F_t(t)$ is the integral over the pulse shape

$$F_t(t) = \int_0^t f(t')\,\mathrm{d}t'. \tag{5}$$

2.2. *Solution of the thermoelastic equation of motion*

For the spherically symmetric case, the thermoelastic equation of motion is given by (Love 1944)

$$\frac{\partial^2 u}{\partial r^2} + \frac{2}{r}\frac{\partial u}{\partial r} - \frac{2u}{r^2} - \frac{1}{c_l^2}\frac{\partial^2 u}{\partial t^2} = \frac{3\lambda + 2\mu}{\lambda + 2\mu}\alpha\frac{\partial \theta}{\partial r}, \tag{6}$$

where $u(r, t)$ is the radial displacement, $c_l = [(\lambda + 2\mu)/\rho]^{1/2}$ is the acoustic wave velocity, λ and μ are the Lame coefficients and α is the coefficient of linear thermal expansion. The initial conditions are

$$u(r, 0) = \frac{\partial u(r, 0)}{\partial t} = 0. \tag{7}$$

For the case of a spherically symmetric temperature distribution, the normal component of the stress tensor is given by Landau and Lifshitz (1986)

$$\sigma_{rr}(r, t) = (\lambda + 2\mu)\frac{\partial u}{\partial r} + \frac{2\lambda}{r}u - (3\lambda + 2\mu)\alpha\theta. \tag{8}$$

For a stress free surface this has to vanish at $r = a$, yielding the boundary condition

$$(\lambda + 2\mu)\left(\frac{\partial u}{\partial r}\right)_{r=a} + \frac{2\lambda}{a}u(a, t) - (3\lambda + 2\mu)\frac{\alpha}{\rho c_h}F_t(t)\sum_{n=0}^{\infty} I_n = 0. \tag{9}$$

For a constrained surface the boundary condition is given by

$$u(a, t) = 0. \tag{10}$$

In view of the linearity of the equation of motion (6), we solve it now for one term of the series (1), and perform the summation over n later. Defining

$$F_r^n(r) = \frac{\mathrm{d}}{\mathrm{d}r}\left[\left(\frac{r}{a}\right)^n\right] \tag{11}$$

$$v_n = \frac{3\lambda + 2\mu}{\lambda + 2\mu}\alpha\frac{I_n}{\rho c_h}, \tag{12}$$

we obtain from equation (6)

$$\frac{\partial^2 u}{\partial r^2} + \frac{2}{r}\frac{\partial u}{\partial r} - \frac{2}{r^2}u - \frac{1}{c_l^2}\frac{\partial^2 u}{\partial t^2} = v_n F_r^n F_t. \tag{13}$$

First, we solve this equation for the case of a step function, $F_t(t) = 1$ for $t > 0$, denoting the corresponding solution $\tilde{u}(r, t)$, and then extend the solution to various pulse shapes using Duhamel's theorem.

We write $\tilde{u}(r, t)$ in the form

$$\tilde{u}(r, t) = \tilde{u}_s(r) + \tilde{u}_t(r, t) \tag{14}$$

so that from equation (13) we obtain

$$\frac{\mathrm{d}^2\tilde{u}_s}{\mathrm{d}r^2} + \frac{2}{r}\frac{\mathrm{d}\tilde{u}_s}{\mathrm{d}r} - \frac{2}{r^2}\tilde{u}_s = v_n F_r^n \tag{15}$$

and

$$\frac{\partial^2 \tilde{u}_t}{\partial r^2} + \frac{2}{r}\frac{\partial \tilde{u}_t}{\partial r} - \frac{2}{r^2}\tilde{u}_t - \frac{1}{c_l^2}\frac{\partial^2 \tilde{u}_t}{\partial t^2} = 0. \tag{16}$$

The boundary conditions at the sphere surface are

$$\tilde{u}_t(a,t) = \tilde{u}_s(a) = 0 \tag{17}$$

for a constrained surface, and

$$(\lambda + 2\mu)\left(\frac{\mathrm{d}\tilde{u}_s}{\mathrm{d}r}\right)_{r=a} + \frac{2\lambda}{a}\tilde{u}_s(a) - (\lambda + 2\mu)v_n = 0 \tag{18}$$

$$(\lambda + 2\mu)\left(\frac{\partial \tilde{u}_t}{\partial r}\right)_{r=a} + \frac{2\lambda}{a}\tilde{u}_t(a,t) = 0 \tag{19}$$

for a free surface.

The general solution of equation (15) can be written in the form

$$\tilde{u}_s(r) = \tilde{u}_{sp}(r) + \frac{D_1}{r^2} + D_2 r, \tag{20}$$

where $\tilde{u}_{sp}(r)$ is a particular solution of equation (15)

$$\tilde{u}_{sp}(r) = \frac{v_n a}{n+3}\left(\frac{r}{a}\right)^{n+1}. \tag{21}$$

From the requirement that $\tilde{u}_s(r)$ should be finite at $r = 0$, it follows that $D_1 = 0$. The coefficient D_2 is obtained from the boundary conditions (17) or (18), yielding the following general solutions of equation (15)

$$\tilde{u}_s^c(r) = \frac{v_n}{n+3}\left[\left(\frac{r}{a}\right)^n - 1\right] r \tag{22}$$

for a constrained surface, and

$$\tilde{u}_s^f(r) = \frac{v_n}{n+3}\left[\left(\frac{r}{a}\right)^n + \gamma\right] r \tag{23}$$

for a free surface. Here

$$\gamma = \frac{4\mu}{3\lambda + 2\mu}. \tag{24}$$

The solution of equation (16) has the form (Lin 1977a)

$$\tilde{u}_t^j(r,t) = \sum_{m=1}^{\infty} B_{mn}^j j_1\left(k_m^j r\right)\cos\left(\omega_m^j t\right), \tag{25}$$

where j_n denotes a spherical Bessel function of order n, $j = c, f$ for constrained and free surfaces, respectively, and

$$\omega_m^j = k_m^j c_l. \tag{26}$$

From the boundary conditions (17) and (19) it follows that k_m^c is the mth root of

$$\tan(k^c a) = k^c a \tag{27}$$

and k_m^f is the mth root of

$$\tan(k^f a) = \frac{4\mu k^f a}{4\mu - (\lambda + 2\mu)(k^f a)^2}. \tag{28}$$

The vibrational frequencies, defined by equation (26), depend only on the sphere size and elastic properties, and not on the heating pattern. The latter determines the relative amplitude

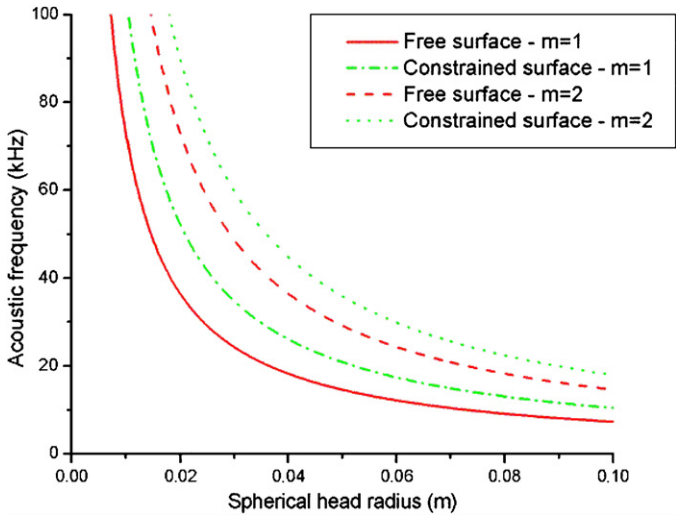

Figure 1. The frequencies of the two lowest acoustic modes, $m = 1, 2$, for free and constrained surface boundary conditions, as a function of the sphere radius.

of excitation of the various vibrational modes. The frequencies of the two lowest order modes, $m = 1, 2$, for both free and constrained surfaces, are shown in figure 1. In all of our numerical calculations we employ the brain matterparameters given by Lin (1977a, 1977b) for the thermal and elastic properties of the sphere. From figure 1 it follows that the microwave hearing effect arises from the excitation of the fundamental mode, $m = 1$. This is because for human head sizes, of radius of about 7 cm, the higher order modes will usually be above the high-frequency auditory limit.

Imposing the initial conditions (7), the coefficients B^j_{mn} are found to have the form

$$B^c_{mn} = \frac{2v_n}{(n+3)\,j_0\left(k^c_m a\right) j_2\left(k^c_m a\right)} \left[\frac{\Lambda_n\left(k^c_m\right)}{a^{n+3}} - \frac{1}{k^c_m}\, j_2\left(k^c_m a\right) \right] \tag{29}$$

$$B^f_{mn} = \frac{-2v_n}{(n+3)\left\{\left[j_1\left(k^f_m a\right)\right]^2 - j_0\left(k^f_m a\right) j_2\left(k^f_m a\right)\right\}} \left[\frac{\Lambda_n\left(k^f_m\right)}{a^{n+3}} + \frac{\gamma}{k^f_m}\, j_2\left(k^f_m a\right) \right], \tag{30}$$

where $\Lambda_n(k)$ is defined as the integral

$$\Lambda_n(k) = \int_0^a x^{n+3} j_1(kx)\,\mathrm{d}x, \tag{31}$$

which can readily be performed analytically.

2.3. Solution for different pulse shapes

Having obtained the solution $\tilde{u}(r, t)$ for the case of a step function, we can now apply Duhamel's theorem (Churchill 1958)

$$u(r, t) = \frac{\partial}{\partial t} \int_0^t F(t - t')\tilde{u}(r, t')\,\mathrm{d}t' \tag{32}$$

to obtain the solution for any pulse shape.

2.3.1. Rectangular pulse. For a rectangular pulse of unit amplitude and width τ, and for a constrained surface, equation (32) yields

$$u^c(r,t) = \sum_{n=0}^{\infty}\left\{\frac{v_n}{n+3}\left[\left(\frac{r}{a}\right)^n - 1\right]rt + \sum_{m=1}^{\infty} B^c_{mn} j_1\left(k^c_m r\right)\frac{\sin\left(\omega^c_m t\right)}{\omega^c_m}\right\} \tag{33}$$

for $0 < t < \tau$, and

$$u^c(r,t) = \sum_{n=0}^{\infty}\left\{\frac{v_n}{n+3}\left[\left(\frac{r}{a}\right)^n - 1\right]r\tau + \sum_{m=1}^{\infty} B^c_{mn} j_1\left(k^c_m r\right)\frac{\sin\left(\omega^c_m t\right) - \sin\left(\omega^c_m (t-\tau)\right)}{\omega^c_m}\right\} \tag{34}$$

for $\tau < t$. Here we have reintroduced the summations over n.

The corresponding solution for a free surface is

$$u^f(r,t) = \sum_{n=0}^{\infty}\left\{\frac{v_n}{n+3}\left[\left(\frac{r}{a}\right)^n + \gamma\right]rt + \sum_{m=1}^{\infty} B^f_{mn} j_1\left(k^f_m r\right)\frac{\sin\left(\omega^f_m t\right)}{\omega^f_m}\right\} \tag{35}$$

for $0 < t < \tau$, and

$$u^f(r,t) = \sum_{n=0}^{\infty}\left\{\frac{v_n}{n+3}\left[\left(\frac{r}{a}\right)^n + \gamma\right]r\tau + \sum_{m=1}^{\infty} B^f_{mn} j_1\left(k^f_m r\right)\frac{\sin\left(\omega^f_m t\right) - \sin\left(\omega^f_m (t-\tau)\right)}{\omega^f_m}\right\} \tag{36}$$

for $\tau < t$.

Having solved for the displacement, we use equation (8) and obtain the radial stress

$$\sigma^j_{rr}(r,t) = \sum_{n=0}^{\infty}\left[v_n G^j_n(r)t + \sum_{m=1}^{\infty} B^j_{mn} k^j_m L^j_m(r)\frac{\sin\left(\omega^j_m t\right)}{\omega^j_m}\right] \tag{37}$$

for $0 < t < \tau$, and

$$\sigma^j_{rr}(r,t) = \sum_{n=0}^{\infty}\left[v_n G^j_n(r)\tau + \sum_{m=1}^{\infty} B^j_{mn} k^j_m L^j_m(r)\frac{\sin\left(\omega^j_m t\right) - \sin\left(\omega^j_m (t-\tau)\right)}{\omega^j_m}\right] \tag{38}$$

for $\tau < t$. Again, $j = c, f$ for constrained and free surfaces, respectively. The functions G and L are defined by

$$G^c_n(r) = -\frac{4\mu(r/a)^n + 3\lambda + 2\mu}{n+3} \tag{39}$$

$$G^f_n(r) = \frac{4\mu}{n+3}\left[1 - \left(\frac{r}{a}\right)^n\right] \tag{40}$$

$$L^j_m(r) = (\lambda + 2\mu) j_0\left(k^j_m r\right) - \frac{4\mu}{k^j_m r} j_1\left(k^j_m r\right). \tag{41}$$

2.3.2. Sawtooth pulse. The pulse is defined by

$$f(t) = \beta t \tag{42}$$

for $0 < t < \tau$, and zero otherwise. Again, we apply (32) to obtain the displacement. From this, the radial pressure is found, using equation (8), yielding

$$\sigma^j_{rr}(r,t) = \sum_{n=0}^{\infty}\left\{\frac{\beta}{2} v_n G^j_n(r) t^2 + \sum_{m=1}^{\infty} B^j_{mn} k^j_m L^j_m(r)\frac{\beta}{\left(\omega^j_m\right)^2}\left[1 - \cos\left(\omega^j_m t\right)\right]\right\} \tag{43}$$

for $0 < t < \tau$, and by

$$\sigma_{rr}^{j}(r,t) = \sum_{n=0}^{\infty}\left\{\frac{\beta}{2}v_n G_n^j(r)\tau^2 + \sum_{m=1}^{\infty} B_{mn}^j k_m^j L_m^j(r)\frac{\beta}{\left(\omega_m^j\right)^2} \times\left[\cos\left(\omega_m^j(t-\tau)\right) - \cos\left(\omega_m^j t\right) - \omega_m^j\tau\sin\left(\omega_m^j(t-\tau)\right)\right]\right\} \tag{44}$$

for $\tau < t$.

2.3.3. Half-sine pulse. The pulse is defined by

$$f(t) = \sin\left(\frac{\pi}{\tau}t\right) \tag{45}$$

for $0 < t < \tau$, and zero otherwise. For the radial pressure we obtain the result

$$\sigma_{rr}^{j}(r,t) = \sum_{n=0}^{\infty}\frac{\tau}{\pi}\left\{v_n\left[1-\cos\left(\frac{\pi}{\tau}t\right)\right]G_n^j(r) + \sum_{m=1}^{\infty} B_{mn}^j k_m^j L_m^j(r) V\left(\omega_m^j,\tau,t\right)\right\} \tag{46}$$

for $0 < t < \tau$, and

$$\sigma_{rr}^{j}(r,t) = \sum_{n=0}^{\infty}\frac{\tau}{\pi}\left\{2v_n G_n^j(r) + \sum_{m=1}^{\infty} B_{mn}^j k_m^j L_m^j(r)\left[V\left(\omega_m^j,\tau,t\right) + V\left(\omega_m^j,\tau,t-\tau\right)\right]\right\} \tag{47}$$

for $\tau < t$, where

$$V(\omega,\tau,t) = \begin{cases} \dfrac{(\pi/\tau)^2}{\omega^2-(\pi/\tau)^2}\left[\cos\left(\dfrac{\pi}{\tau}t\right) - \cos(\omega t)\right] & \omega \neq \dfrac{\pi}{\tau} \\ \dfrac{1}{2}\omega t\sin(\omega t) & \omega = \dfrac{\pi}{\tau}. \end{cases} \tag{48}$$

2.4. Repeated pulses

As long as temperature decay processes may be neglected, which will be the case for a small number of pulses, and not too long intervals between them, the theory can be generalized by a simple superposition of the effects of the separate pulses. Thus, for the general spherically symmetric model, treated in section 2, the radial pressure resulting from N consecutive pulses will be given by

$$\sigma_{rr}^{j}(r,t) = \sum_{n=0}^{\infty}\left\{N v_n G_n^j(r) F_t(t) + \sum_{m=1}^{\infty} B_{mn}^j k_m^j L_m^j(r) \times\left[N F_t(t) + \omega_m^j\sum_{l=0}^{N-1}\int_0^{t-lT}\sin(\omega_m^j(t'-t+lT))F_t(t')\mathrm{d}t'\right]\right\} \tag{49}$$

at the end of the irradiation, i.e., for $t > [(N-1)T + \tau]$. Here T is the time between the beginnings of two consequent pulses, so that the pulse repetition frequency (PRF) is equal to $1/T$. Performing the integration over t' and the summation over ℓ, the following results are obtained from equation (49) for the three pulse shapes defined in section 2.3.

(a) Rectangular pulses

$$\sigma_{rr}^{j}(r,t) = \sum_{n=0}^{\infty}\left\{N v_n G_n^j(r)\tau + \frac{2}{c_l}\sum_{m=1}^{\infty} B_{mn}^j L_m^j(r)\sin\left(\frac{\omega_m^j\tau}{2}\right)\mathrm{Re}\left[\exp\left(\mathrm{i}\omega_m^j(t-\tau/2)\right)W_N^T\left(\omega_m^j\right)\right]\right\}, \tag{50}$$

where

$$W_N^T(\omega) = \frac{1 - \exp(-\mathrm{i}N\omega T)}{1 - \exp(-\mathrm{i}\omega T)}. \tag{51}$$

(b) Sawtooth pulses

$$\sigma_{rr}^j(r,t) = \sum_{n=0}^{\infty} \left\{ \frac{N\beta}{2} v_n G_n^j(r)\tau^2 + \frac{\beta}{c_l} \sum_{m=1}^{\infty} \frac{B_{mn}^j}{\omega_m^j} L_m^j(r) \left[2\sin\left(\frac{\omega_m^j \tau}{2}\right) \right.\right. \\ \left.\left. \times \mathrm{Im}\left(\exp\left(\mathrm{i}\omega_m^j(t - \tau/2)\right) W_N^T\left(\omega_m^j\right)\right) - \omega_m^j \tau \,\mathrm{Im}\left(\exp\left(\mathrm{i}\omega_m^j(t-\tau)\right) W_N^T\left(\omega_m^j\right)\right) \right] \right\}. \tag{52}$$

(c) Half-sine pulses

$$\sigma_{rr}^j(r,t) = 2\sum_{n=0}^{\infty} \left[\frac{N}{\pi} v_n G_n^j(r)\tau - \sum_{m=1}^{\infty} \frac{(\pi/\tau)}{\left(\omega_m^j\right)^2 - (\pi/\tau)^2} B_{mn}^j k_m^j L_m^j(r) \cos\left(\frac{\omega_m^j \tau}{2}\right) \right. \\ \left. \times \mathrm{Re}\left(\exp\left(\mathrm{i}\omega_m^j(t - \tau/2)\right) W_N^T\left(\omega_m^j\right)\right) \right]. \tag{53}$$

3. Comparison with previous analytic models

In previous analytic models (Lin 1977a, 1977b, Shibata *et al* 1986) the spherically symmetric absorption pattern was assumed to exhibit an absorption peak in the centre of the head and to have the form

$$I(r,t) = f(t) I_0 \left[\eta + \frac{\sin(N\pi r/a)}{(N\pi r/a)}(1 - \eta) \right]. \tag{54}$$

Lin (1977a, 1977b) used (54) with $N = 6$ and $\eta = 0$, which has the drawback that the absorbed power is negative in some regions of the sphere. Moreover, even the total absorbed power (obtained by integrating (54) over the sphere volume) is negative. Shibata *et al* (1986) have modified Lin's model by adding the uniform heating term, with $\eta \neq 0$. They used the values $\eta = 0.4$ and $N = 4$, for which the absorbed power is always positive. Also, their choice of η and N yields an absorption pattern which provides a good approximation to that obtained from the exact electromagnetic calculation (Mie theory) for the case of a sphere of radius 0.07 m, which is irradiated by a plane wave of frequency 918 MHz. They have also demonstrated that the introduction of the uniform heating term significantly affects the waveform of the radial stress. We will therefore use the modified Lin model, represented by equation (54), with $\eta = 0.4$ and $N = 4$, as a test case for our general formulation.

The general solution of the equation of motion (6), with the absorption pattern (54) has been derived by Shibata *et al* (1986), using the mathematical techniques presented by Lin (1977a, 1977b). They have solved only for the case of a free surface, and we add here the solution for the case of a constrained surface, which we derived by a similar method. For a rectangular pulse of unit amplitude and width τ, the solution for the displacement has the form

$$u^j(r,t) = u_0 S^j(r) t + \sum_{m=1}^{\infty} A_m^j j_1\left(k_m^j r\right) \frac{\sin\left(\omega_m^j t\right)}{\omega_m^j} \tag{55}$$

for $0 < t < \tau$, and

$$u^j(r,t) = u_0 S^j(r)\tau + \sum_{m=1}^{\infty} A_m^j j_1\left(k_m^j r\right) \frac{\sin\left(\omega_m^j t\right) - \sin\left(\omega_m^j (t-\tau)\right)}{\omega_m^j} \tag{56}$$

for $\tau < t$. Here

$$u_0 = \frac{3\lambda + 2\mu}{\lambda + 2\mu}\alpha\frac{I_0}{\rho c_h} \tag{57}$$

$$S^f(r) = \frac{1-\eta}{N\pi}\left[aj_1(N\pi r/a) - \frac{(-1)^N}{N\pi}\frac{4\mu}{3\lambda+2\mu}r\right] + \eta\frac{\lambda+2\mu}{3\lambda+2\mu}r \tag{58}$$

$$S^c(r) = \frac{1-\eta}{N\pi}\left[aj_1(N\pi r/a) + \frac{(-1)^N}{N\pi}r\right] \tag{59}$$

$$A_m^f = \frac{2u_0 a}{\left[j_1\left(k_m^f a\right)\right]^2 - j_0\left(k_m^f a\right)j_2\left(k_m^f a\right)}$$
$$\times\left\{\frac{(-1)^N}{(N\pi)^2}(1-\eta)\left[\frac{4\mu j_2\left(k_m^f a\right)}{(3\lambda+2\mu)k_m^f a} - \frac{k_m^f a j_0\left(k_m^f a\right)}{\left(k_m^f a\right)^2 - (N\pi)^2}\right] - \eta\frac{\lambda+2\mu}{3\lambda+2\mu}\frac{j_2\left(k_m^f a\right)}{k_m^f a}\right\} \tag{60}$$

$$A_m^c = \frac{(-1)^N}{(N\pi)^2}\frac{2u_0 a(1-\eta)}{j_0\left(k_m^c a\right)j_2\left(k_m^c a\right)}\left[\frac{j_2\left(k_m^c a\right)}{k_m^c a} + \frac{k_m^c a j_0\left(k_m^c a\right)}{\left(k_m^c a\right)^2 - (N\pi)^2}\right]. \tag{61}$$

The radial stress is given by

$$\sigma_{rr}^j(r,t) = u_0 H^j(r)t + \sum_{m=1}^{\infty} A_m^j k_m^j L_m^j(r)\frac{\sin\left(\omega_m^j t\right)}{\omega_m^j} \tag{62}$$

for $0 < t < \tau$, and by

$$\sigma_{rr}^j(r,t) = u_0 H^j(r)\tau + \sum_{m=1}^{\infty} A_m^j k_m^j L_m^j(r)\frac{\sin\left(\omega_m^j t\right) - \sin\left(\omega_m^c(t-\tau)\right)}{\omega_m^j} \tag{63}$$

for $\tau < t$. Here

$$H^f(r) = 4\mu(1-\eta)\left[\frac{(-1)^{N+1}}{(N\pi)^2} - \frac{a}{N\pi r}j_1(N\pi r/a)\right] \tag{64}$$

$$H^c(r) = (1-\eta)\left[(-1)^N\left(\frac{1}{N\pi}\right)^2(3\lambda+2\mu) - \frac{4\mu a}{N\pi r}j_1(N\pi r/a)\right] - \eta(\lambda+2\mu). \tag{65}$$

In order to check the validity of our solutions for the general model (1), we expanded the modified Lin model absorption pattern (54) in a Taylor series. Comparing the solutions (33)–(36) of the general model with the corresponding direct solutions (55) and (56), we note that the calculated coefficients have to obey the relations

$$\sum_n B_{mn} = A_m. \tag{66}$$

We have checked this numerically for the case of a free surface. We have found that for the dominant modes (m values up to 10) equation (66) is satisfied to better than 0.2%, when the Taylor expansion is performed up to $n = 32$. This confirms the validity of the solution of the general spherically symmetric model, as developed in section 2.

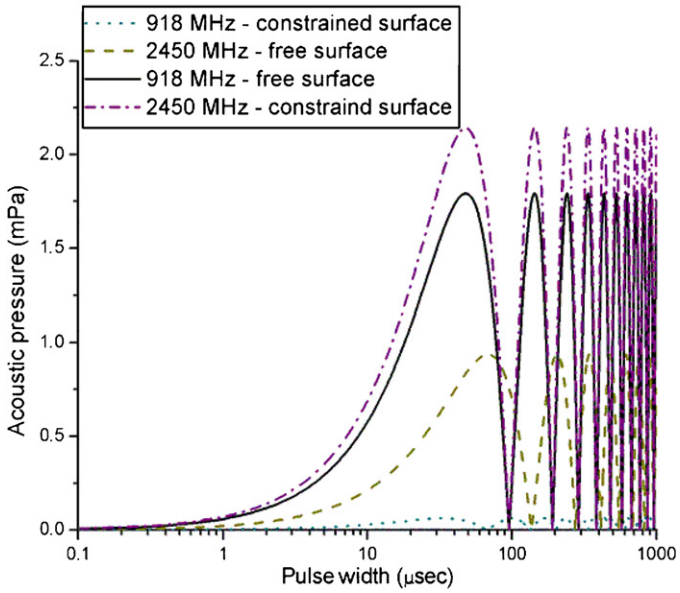

Figure 2. Acoustic pressure, at the head centre, of the fundamental mode as a function of pulse width for different models having the same average SAR of 0.4 W kg^{-1}.

4. Application to a surface concentrated heating pattern

We now apply the general model developed in section 2 to the case in which the absorption of the electromagnetic energy occurs mainly near the surface of the sphere. This is the case for a sphere of radius 0.1 m, and an incident wave frequency of 2450 MHz. We have calculated the absorption pattern for this case, using the Mie theory, and found that the best way to approximate it by a single term spherically symmetric function is to assume that

$$I(r,t) = f(t) I_6 \left(\frac{r}{a}\right)^6. \tag{67}$$

For an incident wave of amplitude 1 W m^{-2}, averaging over the exact heating pattern along the three axes, we find that the optimal value of I_6 is 19 W m^{-3}. Of course, the exact heating pattern is not spherically symmetric, because the absorption near the front surface of the sphere is higher than that near the back surface. However, by using the approximate pattern (67) we will be able to compare the hearing effect due to a surface concentrated heating pattern to the corresponding effect due to a centrally concentrated absorption pattern, equation (54). In order to compare the results obtained with the heating pattern (54), for a sphere of radius 0.07 m, with those obtained with (67), for a sphere of radius 0.1 m, we normalize the amplitudes of the incident waves for the two cases so that they will yield the same average specific absorption rate (SAR), assumed to be equal to 0.4 W kg^{-1}. The dependence of the sound pressure amplitude of the fundamental acoustic mode, at the centre of the head, on the pulse width is shown in figure 2.

The observed oscillatory behaviour of the pressure as a function of the pulse width has been observed experimentally by Tyazhelov *et al* (1979). The oscillatory behaviour has first been predicted by Lin (1977a, 1977b); however according to his model the first peak occurs at a pulse width of about 6 μs. Experimentally, the first peak occurs at 50 μs (Tyazhelov

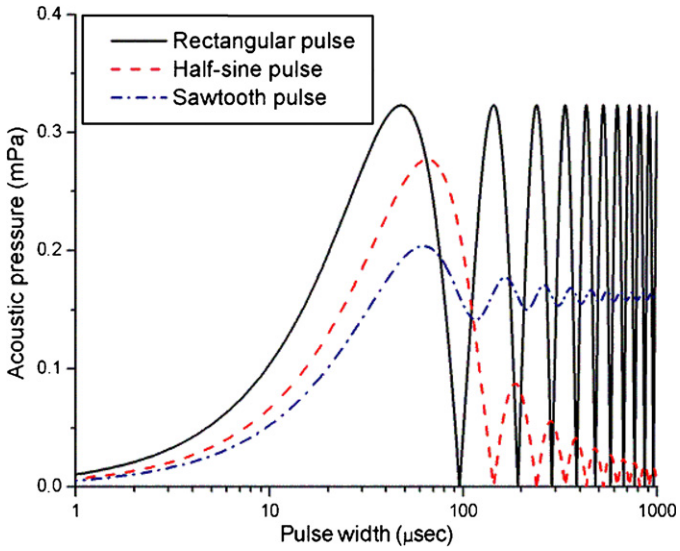

Figure 3. Acoustic pressure, at the head centre, of the fundamental mode as a function of pulse width for three different pulse shapes. The incident wave frequency is 2450 MHz.

et al 1979), which agrees well with our calculation for the modified Lin model (full curve of figure 2). Also, our results demonstrate that, for equal average SAR, the pressure generated by a surface localized heating pattern (2450 MHz) is comparable to that generated by a heating pattern that is peaked at the sphere centre (918 MHz). An interesting difference between the two cases is that for the 2450 MHz case the maximum pressure obtained for a constrained surface is higher than that calculated for a free surface, whereas for the 918 MHz case the free surface yields the larger maximum pressure.

A comparison of different pulse shapes is presented in figure 3. This was calculated for the 2450 MHz case, at the centre of a sphere of radius 0.1 m, with a constrained surface, and an incident power density of 10 W m^{-2}. The rectangular pulse yields the highest maximum pressure, while the sawtooth pulse yields the lowest one. We note that, unlike the cases of the rectangular and the half-sine pulses, for the sawtooth pulse the amplitude of the first acoustic mode does not reduce to zero at higher pulse widths. This is due to the fact that the vanishing of the amplitude results from a destructive interference effect for certain pulse lengths. For the sawtooth pulse, since the pulse amplitude increases over the pulse duration, even when the destructive interference effect operates, it cannot completely annul the acoustic wave amplitude. We also note that the pulse width which maximizes the pressure depends on the pulse shape, being equal to 47.9 μs for the rectangular pulse, to 62.3 μs for the sawtooth pulse and to 65.5 μs for the half-sine pulse.

5. Calculations of PRF dependence

Measurements of the dependence of the hearing effect on the pulse repetition frequency (PRF) have been performed by Tyazhelov *et al* (1979). In their experiments, rectangular pulses of 800 MHz microwaves were coupled via a wave guide from the generator to the parietal area of the head of human observers. Their results for the perceptual threshold as a function of the PRF are shown in figure 4. The two sets of data refer to two observers with high-frequency

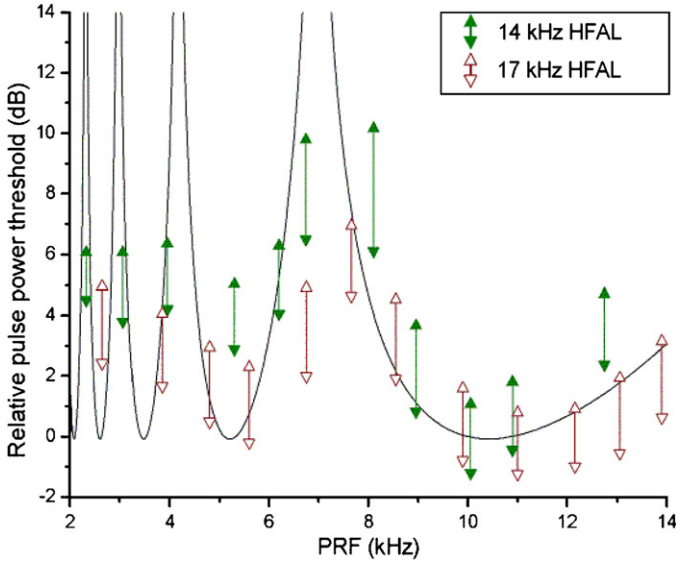

Figure 4. Dependence of the hearing threshold on the pulse repetition frequency. The vertical bars represent the experimental data of Tyazhelov *et al* (1979). The curves have been calculated from the modified Lin model, for two rectangular pulses of 20 μs width.

auditory limits (HFAL) of 14 kHz and 17 kHz. The theoretical results have been obtained by applying equation (50) to the modified Lin model (54), with two rectangular pulses of 20 μs width, and using the free surface boundary conditions. The calculated curves show the ratio of the acoustic pressure induced at the sphere centre at a PRF of 10 kHz to the corresponding pressure at other PRF, expressed in dB. The experimental data have also been normalized to their value at a PRF of 10 kHz. It can be seen that our calculation yields a satisfactory agreement with the experimental data, especially as regards the main feature, i.e., the broad threshold increase around a PRF of about 7 kHz.

6. Conclusion

A generalized analytic model, applicable to an arbitrary microwave absorption pattern of spherical symmetry, has been developed. Whereas in previous analytic models only heating patterns that are peaked at the sphere centre have been considered, we have applied our generalized model to calculate the sound intensity induced by a heating pattern that is concentrated near the sphere surface. We have found that when heating patterns of equal SAR are compared, surface localized and centrally localized patterns yield comparable sound pressures. Another new feature of our model is the allowance for different microwave pulse shapes. This has been applied for comparing the pressure induced by the standard rectangular pulse with those due to the sawtooth pulse and the half-sine pulse. Furthermore, we have extended the theory to the case of repeated pulses, and have found that the calculated dependence of the induced pressure on the pulse repetition frequency provides the first theoretical interpretation of some of the features observed experimentally by Tyazhelov *et al* (1979).

Acknowledgments

The authors would like to thank Menachem Margaliot for helpful discussions.

References

Carslaw H S and Jaeger J C 1959 *Conduction of Heat in Solids* 2nd edn (London: Oxford University Press)

Chou C K, Guy A W and Galambos R 1982 Auditory perception of radio-frequency electromagnetic fields *J. Acoust. Soc. Am.* **71** 1321–34

Churchill R V 1958 *Operational Mathematics* (New York: McGraw Hill)

Elder J A and Chou C K 2003 Auditory response to pulsed radio frequency energy *Bioelectromagnetics* **24** S162–73

Foster K R and Finch E D 1974 Microwave hearing: evidence for thermoacoustic auditory stimulation by pulsed microwaves *Science* **185** 256–8

Frey A H 1961 Auditory system response to radio frequency energy *Aerosp. Med.* **32** 1140–2

Frey A H 1962 Human auditory system response to modulated electromagnetic energy *J. Appl. Physiol.* **17** 689–92

Jin X and Wang L V 2006 Thermoacoustic tomography with correction for acoustic speed variations *Phys. Med. Biol.* **51** 6437–48

Ku G and Wang L V 2000 Scanning thermoacoustic tomography in biological tissue *Med. Phys.* **27** 1195–202

Landau L D and Lifshitz E M 1986 *Theory of Elasticity* (Oxford: Pergamon)

Lin J C 1977a On microwave induced hearing sensation *IEEE Trans. Microw. Theory Tech.* **25** 605–13

Lin J C 1977b Further studies on the microwave auditory effect *IEEE Trans. Microw. Theory Tech.* **25** 938–43

Love A E H 1944 *A Treatise on the Mathematical Theory of Elasticity* (New York: Dover)

Shibata T, Fujiwara O, Katoh K and Azakami T 1986 Calculation of thermal stress inside human head by pulsed microwave irradiation *IEICE Trans. Commun.* **J69-B** 1144–6

Tyazhelov V V, Tigranian R E, Khizhniak E O and Akoev I G 1979 Some peculiarities of auditory sensations evoked by pulsed microwave fields *Radio Sci.* **14** 259–63